FLUID AND SOLID INCLUSIONS IN MINERALS OF THE QUARTZ-CASSITERITE-WOLFRAMITE VEIN "LIDERNAYA", MODOTO ORE DEPOSIT, MONGOLIA: EVIDENCE FOR DISCONTINOUS FLUID EVOLUTION

Christian Schmidt, Ulf Kempe and Serjkhuu Dandar

GeoForschungsZentrum Potsdam, Telegrafenberg A3, 14473 Potsdam, Germany
Freiberg University Mining and Technology Brennhausgasse 14, 09596, Freiberg , Germany
Mongolian University Science and Technology, Ulaanbaatar POBox 46/562, 210646, Mongolia

Introduction

The focus of this study is the fluid evolution in relation to greisen-vein mineralization in the largest Mongolian tin deposit, Modoto. This deposit includes a number of districts with rare-metal mineralizations (Dandar, 1990); the information presented here was obtained using samples from the vein "Lidernaya" in the western part of the Modoto deposit. This vein was selected because it is fairly representative for the primary Sn-W ores in that area, contains a relatively diverse primary mineralization and shows the cross-cutting relationships between quartz-wolframite veins and younger greisen veinlets with cassiterite, topaz, muscovite, and fluorite.

In this study, only primary fluid inclusions were analyzed using microthermometric techniques and Raman spectroscopy because they provide information about the mineralization processes. With the exception of quartz, all host minerals show numerous growth zones; thus, primary inclusions were easily recognizable. Trails of secondary fluid inclusions are abundant particularly in quartz and fluorite. These inclusions were not a subject of this study because it was not possible within a reasonable degree of certainty to relate them to a mineralization event.

Experimental Techniques

Microthermometric measurements of relevant phase changes in inclusions in quartz, topaz, cassiterite, and fluorite were conducted on a Fluid Inc. adapted USGS-type gas-flow heating/freezing stage (Were et al., 1979). An Olympus-BHSM infrared microscope, an infrared TV camera, and a Fluid Inc. adapted USGS-type gas-flow heating/freezing stage modified to allow IR observations was used for the microthermometry of fluid inclusions in wolframite (Luders, 1996).

The thermocouples of both stages were calibrated against the CO_2 triple point (-56.6°C), and the triple point (0.0°C) and critical point of water (374.1°C) using synthetic fluid inclusion standards (Sterner and Bodnar, 1984). The accuracy of the measurements is about ±0.3 to 0.4°C at temperatures of about -60 to 40°C, approximately ±0.1 to 0.2°C for temperatures between -20 and +30°C, and better than ±2 degrees Celsius for temperatures between 100 and 400°C. Temperatures of the following phase transitions were determined during microthermometry of H_2O-NaCl-CO_2-CH_4 inclusions:

(1) the triple point of CO_2, i.e. the melting temperature of solid carbon dioxide in the presence of CO_2 liquid and vapor [Tm(CO_2,s)],
(2) the melting temperature of ice (= freezing point depression) in equilibrium with aqueous liquid and vapor [Tm(ice)],
(3) the dissociation temperature of CO_2 hydrate in equilibrium with aqueous brine, and liquid and vapor carbon dioxide [Tm(CLA)],
(4) the homogenization temperature of the carbonic liquid and vapor phases [Th(CAR)], and
(5) the temperature of total homogenization of vapor and liquid to a single homogeneous phase [Th(L-V)].

Phase transition temperatures (2) and (5) were measured if no carbon dioxide and methane was detected in the inclusions; in these cases, the system for the interpretation of the microthermometric data was simplified to the binary H_2O-NaCl. The salinity of H_2O-NaCl inclusions was calculated based on the equation of Bodnar (1993; his Eqn. 1). Isochore slopes were determined based on measured Th(L-V) and calculated salinities using Eqns. 4, 5, 6, and 7 of Bodnar and Vityk (1994). The pressure at Th(L-V) was calculated using the program MacFlinCor (Brown and Hagemann, 1989).

The system H_2O-NaCl-CO_2±CH_4 was used to interpret the fluid inclusions if significant amounts of volatile components were detected. At low CO_2 concentrations between about 1 and 4 mol% relative to water, the microthermometric and Raman spectroscopic detection limits of in fluid inclusions published by Rosso and Bodnar (1995) were used to estimate the amount of CO_2 in such inclusions. The compositions of H_2O-NaCl-CO_2±CH_4 inclusions were calculated based on microthermometric and Raman-spectroscopic data in conjunction with visual estimation of phase proportions using the program MacFlinCor (Brown and Hagemann, 1989). The melting temperature of solid carbon dioxide in the presence of CO_2 liquid and vapor Tm(CO_2,s) was used to check the purity of the carbon dioxide in the inclusions. The triple point temperature of pure CO_2 is -56.6°C; lower Tm(CO_2,s) indicate the presence of other volatiles such as methane and nitrogen. In this study, Raman spectroscopic analyses showed that lowering of Tm(CO_2,s) was mostly due to methane. The CH_4 content relative to carbon dioxide and an equivalent CO_2 density were calculated based on measured Tm(CO_2,s) and Th(CAR) and the estimated degree of fill with the liquid at Tm(CO_2,s) using the procedure described by Swanenberg (1979). Tm(CLA) data yielded information about the inclusion salinity. For the binary H_2O-CO_2, the clathrate dissociation temperature is 10.0°C, and this temperature decreases as salt is added (Diamond, 1992) and increases with addition of methane (Diamond, 1994). The salinity of H_2O-NaCl-CO_2 inclusions was calculated using the equation of Diamond (1992) relating salinity of the aqueous phase to Tm(CLA) for the univariant equilibrium CO_2 clathrate + CO_2 liquid + vapor + aqueous liquid. A maximum salinity was calculated from Tm(ice) if liquid carbon dioxide was not present at Tm(CLA). The equation of state of Duan et al. (1995) for the NaCl-H_2O-CO_2 system was used to calculate homogenization pressure (= solvus pressure) and isochores based on the measured total homogenization temperature and the calculated bulk composition.

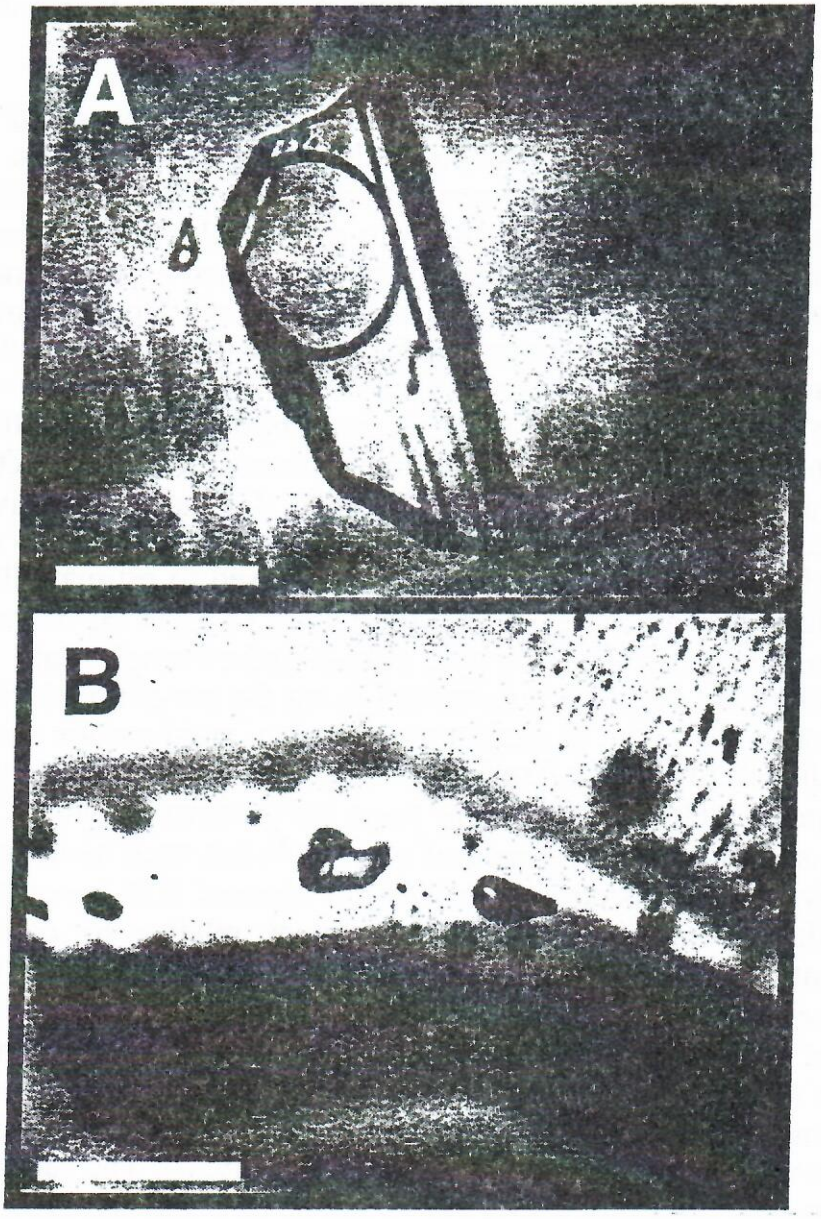

Fig. 1. Transmitted IR light photographs of primary fluid inclusions in wolframite (sample No. 39/4). Scale bar equals 50 μm. A - Large aqueous inclusion showing negative crystal faces. B - Crystallographic orientation of aqueous inclusions parallel to growth zones.

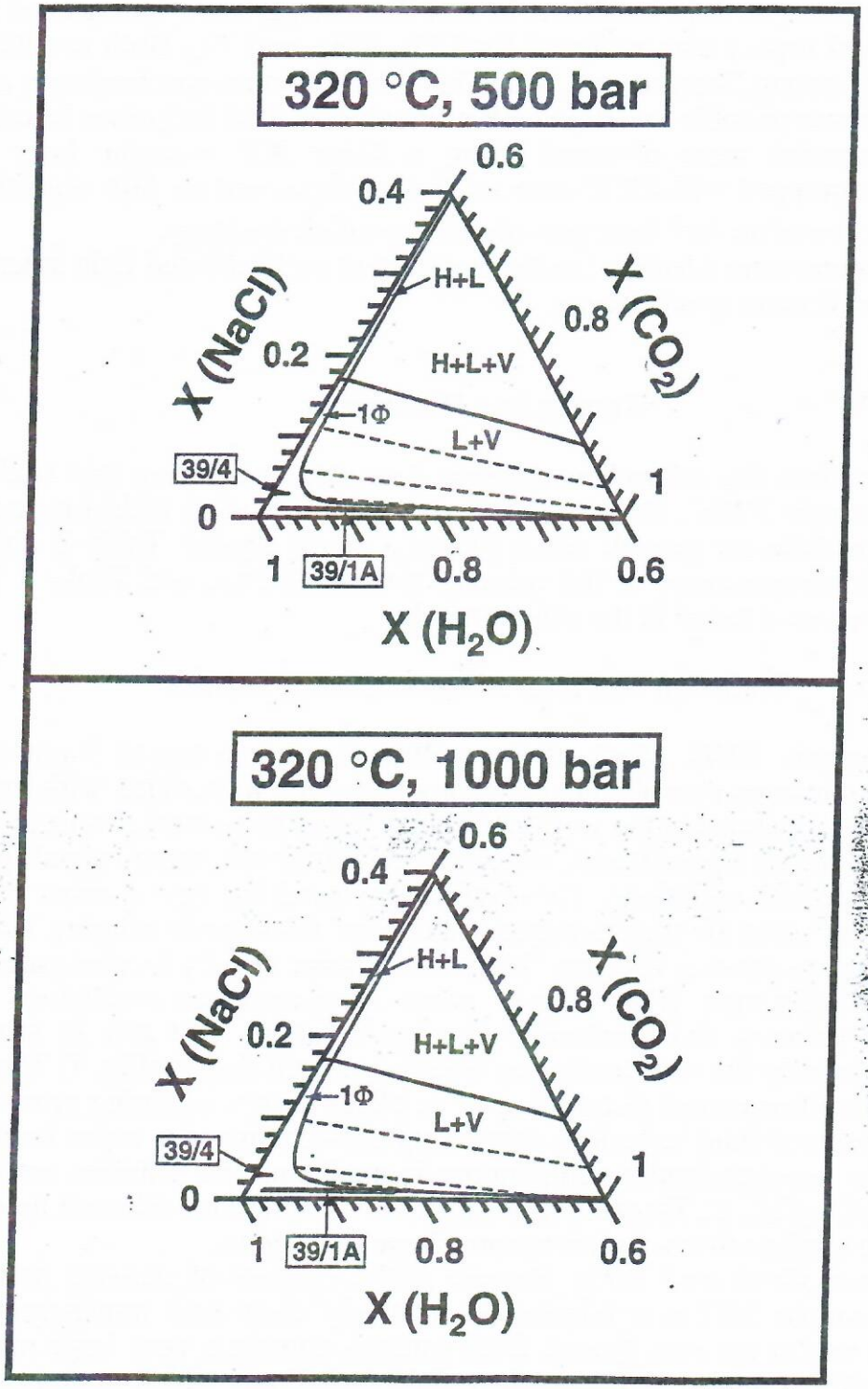

Fig. 2

Fig. 2. Phase diagrams for water-rich compositions in the ternary system H_2O-NaCl-CO_2 at 320°C and 500 and 1000bar. Tielines and solvus location were calculated using the equation of state presented by Duan et al. (1995). 1Φ - one-phase fluid, L+V - coexisting liquid and vapor, H+L - coexisting halite and liquid, H+L+V - coexisting halite, liquid, and vapor. Dotted fields - composition of primary fluid inclusions in wolframite (39/4) and associated massive vein quartz (39/1A).

The vapor phase of fluid inclusions in non-fluorescing hosts transparent to laser light (quartz and topaz) was analyzed for CO_2, CH_4, and N_2. Both cassiterite and fluorite showed strong fluorescence, which hampered Raman spectroscopic analyses; occasionally, it was possible to detect carbon dioxide in fluid inclusions in cassiterite. The Raman spectra were obtained using a Dilor XY modular laser Raman spectrometer, equipped with CCD detector, microscope, and an 80x objective lens. The 514.5 nm line of an Ar^+ laser provided the excitation energy.

Solid inclusions were identified using transmitted and reflected light microscopy, SEM-EDS, and Raman spectroscopy.

Results and Discussion

Table 1 summarizes the microthermometric data obtained during this study. With exception of sample 39/1C, these data were determined using inclusions occurring on two to four different growth zones within a single crystal. Table 2 shows the calculated bulk compositions of the primary fluid inclusions, and Table 3 lists the solid inclusion species found in the vein minerals.

Inclusion and Host Mineral Characteristics

Wolframite (sample 39/4). Much of the wolframite sample (up to 3 cm euhedral tabular wolframite crystals embedded in quartz and some muscovite, with muscovite and quartz filling fractures in the wolframite) was found to be transparent to infrared light. However, the IR transmittance was different within the same crystal, probably due to compositional variations. The sample displayed a large number of zones having about the same IR transmittance which had thicknesses ranging between a few micrometers to several 100 μm. These zones were usually located parallel to a crystallographic direction (Fig. 1) and were interpreted as oscillatory growth zonation. The primary fluid inclusions are up to about 100 μm in size, fairly isometric to relatively flat and can display negative-crystal shapes (Fig. 1) They occur in random three-dimensional distribution or in planar arrays outlining growth zones (Fig. 1). All observed fluid inclusions contain aqueous liquid and a vapor bubble. The variation of the homogenization temperature is small, and the salinities are close to 10 wt% eq. NaCl (Tab. 1). Freezing runs indicated the presence of small amounts of carbon dioxide and/or other volatiles in some large inclusions.

Quartz (samples 39/1A and 39/2). Sample 39/1A consists of massive milky-white vein quartz, sample 39/2 is a terminared relatively clear and transparent quartz crystal from a vug in the vein quartz. Both samples contain a very large number of primary, pseudosecondary, and secondary fluid inclusions, which contain aqueous liquid and a vapor phase. Additionally, many inclusions contain a liquid CO_2 phase at room temperature. The carbon dioxide concentrations and the densities of the CO_2-rich phase at Th(CAR) vary in wide ranges, while the salinity is relatively constant (cp. Tab. 1, Tab. 2., Fig. 3). Methane and, occasionally, traces of nitrogen were detected using Raman spectroscopy. Postentrapment volumetric and compositional modifications ("necking-down" (Roedder, 1984)) are evident for most inclusion groups. Such inclusions were not selected for microthermometric measurements. A

Table 1. Microthermometric data for primary inclusions in minerals from the vein "Lidernaya", Modoto, Mongolia

Sample No./ Mineral	Tm(CO_2, s) [°C]	Tm(ice) [°C]	Tm(CLA) [°C]	Salinity [eq. wt% NaCl]	Th(CAR) [°C]	Vf(CAR) at Th(CAR)	Th(L-V→L) [°C]
39/1A massive milky-white vein quartz	-57.0 (-57.5 - -56.8) n=7	-4.6 (-4.9 - -4.1) n=7	8.6 (8.5 - 8.8) n=7	3 - 4 (est) > 2.8 (2.4 - 3.0) (2) < 7.3 (1)	15.0 (V) - 22.5 (L) n=7	0.2 - 0.4	279 (263 - 294) n=7
39/1B euhedral cassiterite	n.o.	-2.7 (-2.8 - -2.6) n=5	n.o.	4.5 (4.3 - 4.6) (1)	n.o.	—	332 (328 - 334) n=10
	n.o.	-2.7 n=1	-1.6* n=1	—	n.o.	—	328 n=1
39/1C corroded inclusions of quartz in cassiterite	n.o.	-6.5 n=1	n.o.	9.9 (1)	n.o.	—	465 (C) n=1
39/2 terminated quartz crystal, relatively clear	-57.4 (-57.7 - -56.8) n=14	-3.7 (-4.7 - -3.0) n=14	10.3 (9.4 - 10.8) n=14	2 - 4 (est) < 6.0 (1)	5.0 (V) - 26.3 (L) n=14	0.2 - 0.4	271 (243 - 302) n=14
39/3 terminated fluorite crystal from cavity, transparent, whitish, purple growth zones	n.o.	-0.6 (-1.6 - -0.2) n=7	n.o.	1.0 (0.4 - 2.7) (1)	n.o.	—	160 (144 - 176) n=7
39/4 wolframite, euhedral	n.o.	-6.1 (-6.2 - -6.0) n=3	n.o.	9.3 (9.2 - 9.5) (1)	n.o.	—	320 (314 - 327) n = 11
	(-106 - -76)* n = 3	(-10.1 - -7.2) n=3	(-3.1 - -2.5)* n=3	—	n.o.	—	323 (318 - 325) n = 3
39/5 cassiterite associated with muscovite and quartz	n.o.	-2.6 (-2.7 - -2.5) n=6	n.o.	4.3 (4.2 - 4.5) (1)	n.o.	—	334 (331-336) n=15
39/6 pale yellow terminated topaz crystal	n.o.	-2.6 (-2.9 - -2.3) n=6	n.o.	4.3 (3.9 - 4.8) (1)	n.o.	—	330 (329-331) n=6
	(-56.6 - -56.9) n=3	(-2.0 - -1.8) n=3	8.8 (8.7 - 9.1) n=3	2.4 (1.8 - 2.6) (2)	13.0 (V) - 14.0 (V) n=3	0.3	326 (324 - 327) n=4

$Tm(CO_2, s)$ = average melting temperature of solid carbon dioxide in equilibrium with liquid CO_2 and vapor; Tm(ice) = average melting temperature of ice; Tm(CLA) = average dissociation temperature of CO_2 hydrate in equilibrium with aqueous brine and liquid and vapor carbon dioxide; Salinity = average equivalent NaCl concentration of the solution in weight percent relative to H_2O; (1) calculated using the equation relating freezing point depression and salinity for aqueous NaCl solutions up to 23.2 wt% NaCl from Bodnar (1993); (2) calculated using the equation from Diamond (1992) relating salinity of the aqueous phase to Tm(CLA) for the univariant equilibrium CO_2 clathrate + CO_2 liquid + vapor + aqueous liquid; Th(CAR) = homogenization temperature of the carbonic liquid and vapor phases; (L) = homogenization to the liquid CO_2 phase; (V) = homogenization to the vapor CO_2 phase; Vf(CAR) at Th(CAR) = volume fraction of the carbonic phases at Th(CAR); $Th(L+V \rightarrow L)$ = average liquid-vapor homogenization temperature (total homogenization to the liquid, aqueous phase); (C) = total homogenization by critical behavior; n.o. = not observed; * = no liquid CO_2 present; (numbers in parenthesis) = the range in measured temperatures; n = number of inclusions measured; (est) = estimated

reliable identification of primary inclusions was difficult due to the scarcity or absence of growth zones in the quartz samples; most of the empirical criteria for primary origin of fluid inclusions listed by Roedder (1984) were not applicable to these samples. Isolated inclusions which were also usually more mature than secondary inclusions on healed fractures, and inclusions that were located in small groups parallel to a crystal face and did not show significant "necking-down" were taken as probably of primary origin and used to determine approximate densities and compositions of the quartz-forming fluid.

Corroded quartz inclusions in cassiterite (sample 39/1C). This quartz contains primary fluid inclusions that are clearly different from any other observed type of fluid inclusions. The inclusions are very small (less than 10 μm) and have negative crystal shapes. The room temperature liquid-vapor phase ratio appeared to be relatively constant. Only one inclusion had a sufficient size to be used for an accurate microthermometric analyses. It homogenized by critical behavior, at a much higher temperature than any other inclusion analyzed in this study (Tab.1, Fig. 3). Using the equations presented by Knight and Bodnar (1989) relating salinity and critical temperature of NaCl-H_2O solutions, the determined salinity was found to be in agreement with the measured critical homogenization temperature.

Topaz (sample 39/6). The sample consisted of a pale-yellow terminated isometric crystal of about 5 mm in diameter. The topaz displays numerous several tens to a few hundred μm thick growth zones parallel to the c axis, particularly close the rims of the crystal; sectoral zoning prevails in the core. The zonation is best visible in polarized light. At least some of the sectoral and growth zoning appears to be caused by changes in the fluorine content of the topaz (Fig. 5). Some growth zones are partly outlined by primary fluid inclusions. The inclusions were up to 250 μm in their longest dimension. At room temperature, all inclusions in the sample display an aqueous liquid phase and a vapor bubble. When the sample was cooled below room temperature, small amounts of a liquid CO_2 phase were visible in some of the larger inclusions while no condensation of liquid carbon dioxide was observed in other inclusions. Raman spectroscopy of the vapor bubbles showed the occasional presence of small amounts of methane, and a variable CO_2/CH_4 ratio. There is very little scatter in Th(L-V) of inclusions on the same growth zone, and no significant differences in homogenization temperature and salinity were found for inclusions located on different growth zones. Composition and homogenization temperature of primary fluid inclusions in topaz and cassiterite are similar (cp. Tab. 1, Tab. 2, and Fig. 3); both minerals were probably deposited about the same conditions.

Furthermore, the fluid inclusions contain two different, very small (less than about 5 μm) solids which were not close enough to the sample surface for an identification using Raman spectroscopy. One of these solids is opaque and black (possibly an oxide), the other solid is birefringent and reddish-yellowish in polarized light. Both solids show no signs of dissolution during heating to 350°C.

Cassiterite (samples 39/1B and 39/5). Both samples contained euhedral to subhedral, roughly isometric cassiterite crystals up to 2 cm in diameter which were partly associated with quartz (sample 39/1A), muscovite, and topaz. The cassiterite is reddish to orange brown to light yellowish brown in transmitted light, and shows slight, but pronounced pleochroism. Sample 39/1B exhibits a very distinct combined sector and (101) + (100) oriented color zoning. The cassiterite contains frequently

blebs and rods of a Ti oxide (rutile?) with significant Fe, Nb, and W contents (Tab. 3). The Ti-oxide inclusions occur along fractures (these should have formed later than the host) in the cassiterite or are isolated (these can be exsolutions or a result of epitaxial growth during cassiterite formation). Topaz, quartz (sample 39/1C), a Ti-Fe-Mn mineral, and possibly muscovite were also observed as solid inclusions in cassiterite (Tab. 3).

A large number of primary and pseudosecondary fluid inclusions (aqueous, liquid-rich) occurs in both cassiterite samples. Secondary inclusions are rare. The primary fluid inclusions are located along color zones and twin planes and are up to about 100 μm in size. The determined homogenization temperatures and salinities of primary fluid inclusions display very little variation (Tab. 1). The vapor bubbles contain some carbon dioxide, but the CO_2 density was too low to form a liquid CO_2 phase upon cooling. Clathrate melting was visible in a very large inclusion. Although the samples were fluorescent, Raman spectra of the vapor bubbles showed occasionally peaks at about 1388 cm^{-1} and 1285 cm^{-1} which are characteristic for carbon dioxide (ν_1-$2\nu_2$ Fermi diad of CO_2). Very small insoluble daughter phases were observed in many of the larger inclusions. These daughter phases are very similar to those occurring in primary fluid inclusions in topaz.

Fluorite (sample 39/3). The sample shows relatively thin (less than about 0.5 mm) purple growth zones in an otherwise colorless to whitish fluorite. These purple color zones are mostly located near or at the crystal faces. Primary inclusions are often located have generally negative crystal shapes and contain aqueous liquid and vapor, with apparently quite constant liquid to vapor ratios, although there is some scatter in the Th(L-V) of the primary fluid inclusions. Both salinity and homogenization temperature are significantly lower than those of primary fluid inclusions of any other sample (Tab. 1). If volatiles are present, their concentration is below the detection limits of microthermometry. Raman spectroscopic analyses were not carried out due to the strong fluorescence of the sample.

Dandar (1990) reported results of crush-leach analyses (?) of fluid inclusions in cassiterite and quartz from the Bayanmod tin deposit, Modoto. The reported solute concentrations show that Na^+, K^+, HCO_3^-, and Cl^- are the prevalent ions which suggests a granitic source of the mineralizing fluids. Li^+, Ca^{2+}, Mg^{2+}, and F^- are present in lower concentrations compared to Na^+, K^+, HCO_3^-, and Cl^-. These results are consistent with the observed approximate temperatures of first ice melting observed in this study (generally less than -28°C and mostly about -20 to -22°C for all samples), which indicate that $CaCl_2$ and $MgCl_2$ are not a major component in the fluid. Thus, it is reasonable to assume that the interpretation of the fluid inclusion data obtained in this study can be based on an approximation of by. systems H_2O-NaCl and H_2O-NaCl-CO_2. However, quantitative data for solute concentrations in fluid inclusion liquids obtained using crush-leach techniques should be used with caution; they are often unreliable due to the inherent problems during release, extraction, and analysis of the fluids (Roedder, 1984). Assuming that possible analytical errors can be ignored, the compositions given by Dandar (1990) can be applied to estimate the fluid compositions at the vein "Lidernaya", because:

1) the vein "Lidernaya" is one source of the placer Bayanmod,
2) petrographic characteristics, homogenization temperatures, and salinities of fluid inclusions in cassiterite, topaz, and quartz from the vein "Lidernaya" are very similar to those of other veins in the Bayanmod district (Schmidt and Leeder, 1992), and
3) secondary inclusions in cassiterite (and topaz) are rare; data for the fluid composition obtained from a bulk cassiterite (or topaz) sample should reflect the composition of the primary, mineral-forming, greisen fluid.

Paragenetic Sequence at the Vein "Lidernaya"

The paragenetic sequence was obtained by combining petrographic and field observations with the evidence provided by solid and fluid inclusions. Other interpretations than the one given here are possible which are equally consistent with the petrographic and inclusion data, e.g. it is not clear if the quartz inclusions in cassiterite formed at an early stage of greisen veinlet mineralization or during a separate fluid event. The following paragraphs describe a probable mineralization sequence at the vein "Lidernaya" based mainly on the evidence available in this study.

1 - Quartz-wolframite stage. The first mineral assemblage at the vein "Lidernaya" consists of wolframite, followed by muscovite, massive milky-white vein quartz and relatively clear terminated quartz crystals in vugs. The vein quartz contains small amounts of a euhedral needle-shaped mineral, possibly rutile or tourmaline.

2 - Corroded quartz preserved as inclusions in cassiterite. The fluid inclusions characteristics distinguish this quartz type clearly not only from the quartz deposited during the quartz-wolframite stage but they are also different from any other observed type of fluid inclusions. The microthermometric and petrographic results of the inclusion studies also show that is unlikely that any of the quartz samples was in equilibrium with wolframite, topaz, or cassiterite. The quartz inclusions in cassiterite are interpreted here as relicts of an early high-temperature mineralization from a magmatic fluid which had exsolved during the crystallization of a relatively shallow granite intrusion which occured after the formation of the quartz-wolframite veins. Most of that high-temperature quartz was then dissolved by greisen fluids, but a small amount was trapped as solid inclusions in cassiterite.

3 - Greisen veinlets. The quartz-wolframite veins are cut by greisen veinlets, containing muscovite, topaz, and cassiterite. Primary fluid inclusion characteristics of topaz and cassiterite are similar, which indicates both minerals were probably deposited at about the same conditions. Muscovite occurs as inclusions in topaz, and the cassiterite contains topaz (and muscovite?) inclusions (Tab. 3). Thus, at least some of the muscovite formed before topaz precipitated, and at least some topaz was already present when cassiterite formed. A Fe, Nb, and W bearing Ti-oxide (rutile?) was deposited during and/or after cassiterite.

Ivanova (1976) distinguishes a sulfide stage (including pyrite, arsenopyrite, sphalerite, chalcopyrite, and galena) between an early cassiterite-wolframite and a late quartz-fluorite stage in the paragenetic sequence of the Sn-W veins at the Modoto deposit. No confirmation can be given here due to the lack of sulfides in the collected samples from the surface outcrop of vein "Lidernaya".

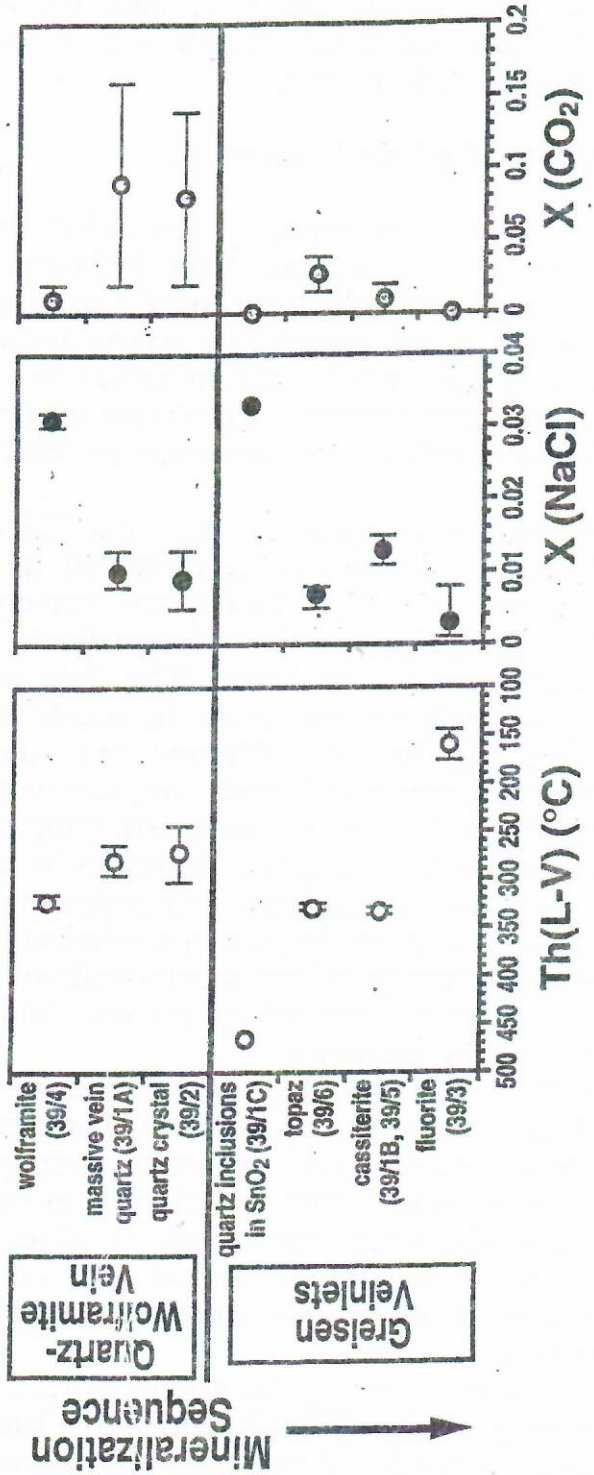

Fig. 3. Variation of homogenization temperature and composition of primary fluid inclusions with the paragenetic sequence of the vein "Lidernaya", Modoto, Mongolia. Th(L-V) - total liquid-vapor homogenization temperature, X (NaCl) - salinity expressed as mole fraction NaCl in the bulk fluid based on the determined eq. wt% NaCl (Tab. 1 and Tab. 2), X (CO_2) - mole fraction carbon dioxide in the fluid bulk composition.

4 - Late-stage open-space deposition. Fluorite is one of the youngest hydrothermal minerals in the vein "Lidernaya" and occurs in vugs and cavities in the greisen veinlets. The low salinities and volatile concentrations in the primary fluid inclusions can indicate dilution of the magmatic greisen fluids by influx of meteoric waters. However, there are no isotopic data which could support or contradict this statement. Reactivation of the vein structure and deposition of the fluorite during a separate event is another possibility. In any case, the fluorite should have formed at temperatures (probably less than about 250 °C) which were significantly lower compared to those present during the first three stages (probably about 400 °C or above).

Fluid evolution and Mineral Formation Conditions

No petrographic and microthermometric evidence was observed that boiling fluids occurred at any stage of mineral deposition in the vein. Therefore, all studied inclusions trapped (originally) a one phase fluid. Furthermore, significant postentrapment modifications of the fluid inclusions resulting in compositional and density variations occurred only in the quartz samples 39/1A and 39/2. Consequently, the pressures and temperatures during vein mineralization were above the liquid-vapor curve pressures and temperatures corresponding to the isochores of the primary fluid inclusions in all samples (with the possible exception of 39/1A and 39/2), and a pressure correction is required to obtain formation temperatures (cp. Roedder, 1984). However, geologic observations show that the vein-mineralizing hydrothermal systems at the Modoto deposit were relatively shallow (some veins at the Modoto deposit are hosted by granite which cuts unmetamorphosed Permian sediments (Dandar et al., 1979; Dandar, 1990); furthermore, the vein "Lidernaya" contains many cavities and vugs). It is estimated here that the pressures during vein mineralization did probably not exceed about 2 kbar. "Overpressures" in excess of the lithostatic pressures may occur due to the increase in vapor pressure during crystallization of a granitic magma but should quickly decrease due to volcanism and/or fracturing of the granite roof rocks; thus, presence of significant fluid overpressures at the time of the vein mineralization appears to be unlikely.

In the one-phase field of a fluid system, formation temperatures must be known to calculate formation pressures from determined isochores. In this study, relatively large intervals of reasonable crystallization temperatures were estimated because applicable independent geothermometers were not available for most samples. For brevity, only the example of fluorite (sample 39/3) is given here to illustrate how a reasonable crystallization temperature interval was estimated. Fluorite formation temperatures above about 250 °C are unlikely due to the relatively shallow geologic environment and the steep isochores of the primary fluid inclusions in a P-T plot. A formation temperature of just 300 °C would imply pressures at fluorite deposition of about 2.4 kbar, and a formation temperature of 400 °C would require pressures in excess of 4 kbar, which is not consistent with the geologic observations. on the other hand, the fluorite crystallized in the one-phase field of the mineralizing fluid, i.e. formation temperature was above the homogenization temperature (144°C to 176°C). Therefore, the fluorite crystallization temperature was most likely approximately 200 °C, and a formation temperature interval between about 180°C

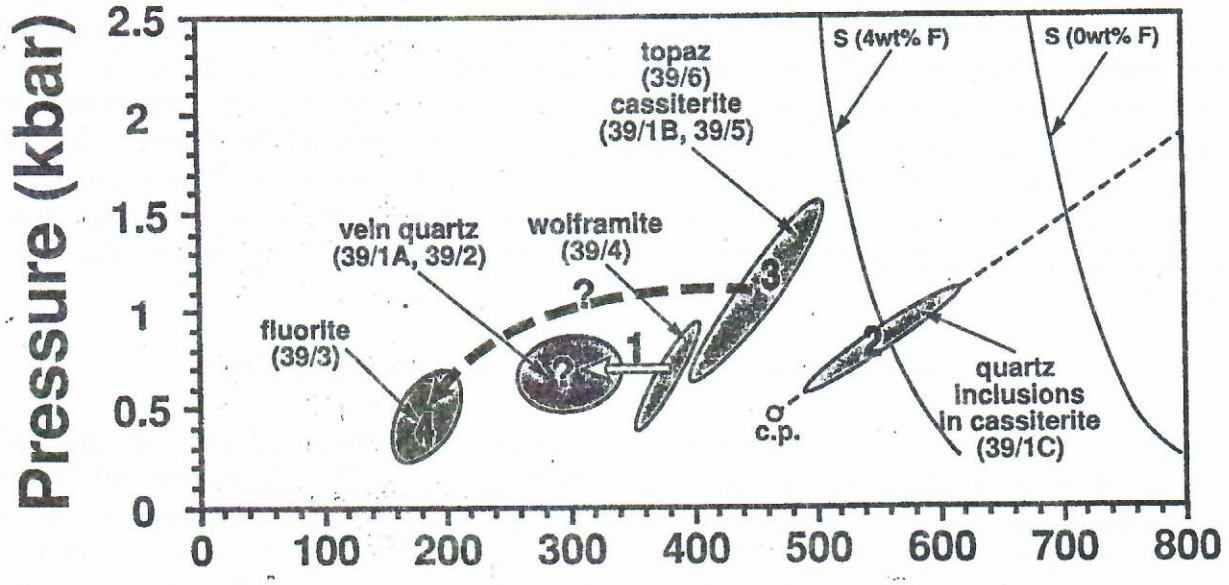

Fig. 4. P-T evolution of the vein "Lidernaya", Modoto deposit, based on determined isochore locations and formation temperature estimates. The postmagmatic mineralisation starts after granite solidification. S (0 wt% F) - water-saturated granite solidus (from Burnham, 1979), S (4 wt% F) - water-saturated solidus curve of a granite containing 4 wt% fluorine (Thomas, 1994), c.p. - critical point of a H_2O + 10 wt% NaCl solution and corresponding critical isochore (dashed line); probable mineralization sequence: 1 - quartz-wolframite stage, 2 - corroded quartz preserved as inclusions in cassiterite, 3 - greisen veinlets containing muscovite, topaz, and cassiterite, 4 - late stage open-space deposition (fluorite); numbers in parenthesis - sample numbers.

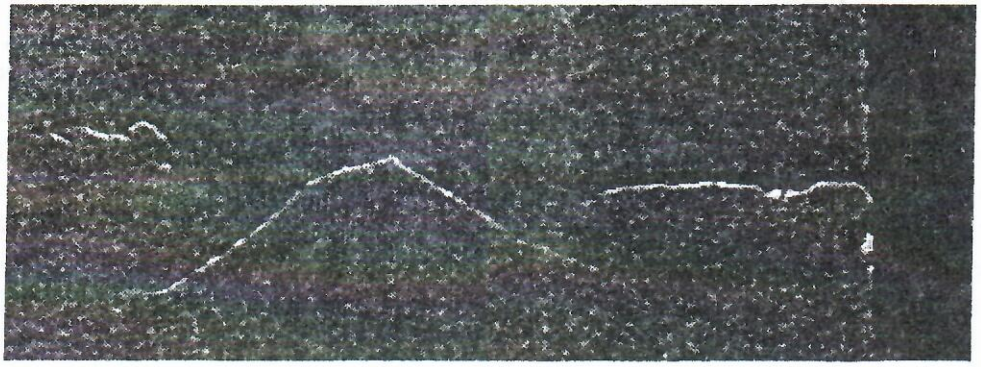

Fig. 5. Microprobe image of fluorine distribution in topaz (sample 39/6). Higher fluorine concentrations are brighter. Field of view width equals 1 mm.

to 250°C was assumed. Tab. 4 lists calculated pressures based on such estimated formation temperature intervals, and Fig. 4 shows a model of the P-T evolution during the mineralization of the vein "Lidernaya" inferred from microthermometric data obtained in this study and the geologic and petrographic evidence.

If an inclusions trapped a fluid immediately after exsolution from a granitic source, intersection of the isochores corresponding to the molar volume of the inclusion with an applicable granite solidus provides a formation pressure. This approach can only yield reliable data if the inclusions were trapped at a temperature close to the granite solidus temperature because it cannot be assumed that the P-T path during cooling of the exsolved granitic fluids in the hydrothermal system is constrained by a constant molar volume of the fluid. In this study, application of this technique yielded a reasonable pressure for inclusions in sample 39/1C (corroded quartz inclusions in cassiterite) which display the highest minimum formation temperature (homogenization temperature). Extrapolation of the inclusion isochores of any other sample to the solidus temperature of a granite containing 0 to 2 wt% F results in pressures above 2 kbar.

Another estimate for a maximum formation temperature of sample 39/1C can be derived from the observation that the primary inclusions displayed negative-crystal shapes of typical α-quartz morphology. The α/β quartz inversion line and the isochore intersect at about 600°C and 1030 bar. The formation conditions of sample 39/1C should be below that temperature and pressure (if the assumption is valid that the inclusion morphology can be taken as an indication for crystallization in the α-quartz field), but above 465°C and about 460 bar, which are the minimum formation conditions derived from homogenization temperature and pressure (Tab. 4). Fluids that formed earlier quartz in the quartz-wolframite veins (samples 39/1A and 39/2) were much cooler and denser and were compositionally different (lower salinity, higher carbon dioxide concentrations). This indicates a discontinuity in the fluid evolution due to the influx of a new, high-temperature fluid (very likely from a granitic source) into the vein structure after crystallization of the quartz-wolframite assemblage (Fig. 4).

Previous studies of fluid inclusions in wolframite and coexisting quartz showed significant differences in inclusion and, often, homogenization temperature (Campbell and Panter, 1990; Lüders, 1996). The following possibilities were discussed to explain the compositional distributions (cp. Lüders, 1996):

1) precipitation of quartz and wolframite was contemporaneous and a result of boiling,
2) the precipitation of quartz and wolframite was not contemporaneous; boiling of the fluid at depth occurred prior to wolframite deposition,
3) the formation of quartz and wolframite was caused by different fluids.

In this study, the fluid inclusions in quartz and wolframite from the vein "Lidernaya" are, likewise, different with respect to salinity, CO_2 concentration, and homogenization temperature. The inclusion compositions were plotted in two ternary diagrams at constant temperature (320°C) and pressures of 500 and 1000 bar (Fig. 2). The ternary diagrams include phase equilibria and tielines in the liquid-vapor field in the system H_2O-NaCl-CO_2. The selected temperature of 320°C results from the assumption of possible immiscibility, i.e. if wolframite has formed due to

boiling, the lowest Th(L-V) of the primary fluid inclusions in wolframite can (theoretically) be taken as the formation temperature.
Contemporaneous precipitation of quartz and wolframite as a result of boiling can be excluded. The composition of the inclusions are within the one-phase field. Even if the immiscibility boundary would extend to the composition of the wolframite forming fluids and the composition of primary fluid inclusions in coexisting quartz, both compositions would not be connected by a tieline at any pressure (Fig. 2). Furthermore, wolframite contains only aqueous fluid inclusions, and the occurrence of vapor-rich H_2O-CO_2 inclusions was only observed in the quartz samples. There is no obvious reason for a compositionally selective trapping of fluid inclusions in wolframite and quartz if one assumes their coprecipitation in a boiling fluid, unless the wolframite sample formed in deeper parts of the vein and trapped the more dense aqueous fluid and the quartz samples formed in shallower parts of the vein and trapped the less dense CO_2-rich phase. However, all 3 samples were taken at the same surface outcrop of the vein.
The second possibility (boiling of the fluid at depth occurred prior to wolframite deposition) is also unlikely. An increase in pressure would expand the one-phase field. Thus, the pressure would have to be significantly below 500 bar. Unfortunately, the existing equations of state for the system H_2O-NaCl-CO_2 are not reliable at these pressures. Therefore, the following argument is based on an extrapolation of the trend of the tieline slopes with decreasing pressure from the known tielines between 500 and 1000 bar. For any bulk composition that could be located on a tieline connecting the composition of the fluid inclusions in wolframite and quartz, the composition of the coexisting CO_2-rich vapor phase shifts rapidly towards higher $X(CO_2)$ with *decreasing* pressure whereas X(NaCl) approaches zero, i.e. the inclusions in quartz contain too much NaCl and not enough carbon dioxide to be in equilibrium with composition of the fluid inclusions in wolframite. Furthermore, if boiling had occurred at depth, the exsolving less dense CO_2-rich vapor phase should be the first phase to rise towards shallower parts of the vein and at least some quartz would precipitate before wolframite formation from the more dense and saline aqueous fluid. However, there is no petrographic evidence that quartz was deposited prior to wolframite.
Therefore, it is unlikely that both fluids were in equilibrium or evolved from a parent fluid due to immiscibility, unless mixing with other fluids is invoked. Meteoric water would be a likely second fluid source; mixing with meteoric water should be reflected in a compositional shift towards the H_2O-corner of the ternary diagram and can explain the location of the compositional fields of primary fluid inclusions in wolframite and associated massive vein quartz (Fig. 2). However, this explanation still implies formation of some quartz prior to wolframite, and no proof of that can be given here. A much simpler interpretation is that wolframite and quartz at the vein "Lidernaya" precipitated from two different fluids, during two temporally separate mineralization events, which is also consistent with the petrographic observations.

Raman spectroscopy of the volatiles in fluid inclusions in topaz showed that the CO_2/CH_4 ratio is variable, which indicates that the hydrogen fugacity in the

hydrothermal fluid was not fixed during topaz formation. The topaz displays fine growth zones parallel to the c axis; these can not be explained by pressure changes due to opening and closing of the vein and some concomitant pressure variation between hydrostatic and lithostatic conditions, because there was very little change in fluid density during topaz deposition as reflected by the very small range in total homogenization temperatures of the fluid inclusions. Furthermore, there is no fluid inclusion evidence for the occurrence of boiling. Therefore, the fine growth zonation was caused by some different mechanism; the "oscillating" changes in hydrogen fugacity could perhaps be due to numerous successive events of fluid influx into the veinlets from the same source (exsolved fluid from a crystallizing granitic magma), but this explanation is rather speculative.

Fine growth zoning is also characteristic for the cassiterite and wolframite samples. The range in Th(L-V) of fluid inclusions in both minerals is very similar to that of the fluid inclusions in topaz. Thus, it is not unreasonable to assume that the growth zoning of wolframite and cassiterite is, likewise, caused by oscillations in fH_2.

The presence of small amounts of methane in fluid inclusions in quartz and topaz (and, likely, cassiterite) indicates slightly reducing conditions during the precipitation of these minerals.

Cline and Bodnar (1991) presented results of numerical simulations of chlorine partitioning between a crystallizing granitic melt and exsolving aqueous fluids. At pressures of 0.5 and 1 kbar, an initial water content of 2.5 wt% in the melt, and an initial Cl/H_2O ratio of 0.1, the first exsolving fluids have a low salinity and the salinity increases as crystallization progresses. However, the first fluid exsolved from a granitic melt at 2 kbar pressure (but the same initial water content and Cl/H_2O ratio) has a high salinity (more than 50 wt% NaCl), the fluid salinity decreases as crystallization of the melt proceeds and approaches zero at completion of the crystallization process.

Fig. 3 shows the variation of homogenization temperature and composition of primary fluid inclusions with the paragenetic sequence of the vein "Lidernaya". The fluid evolution in both the earlier quartz-wolframite assemblage and the later greisen veinlet assemblage is characterized by a salinity decrease with time. This is not consistent with the shallow intrusion level of the granites at the Modoto deposit, if one assumes that all involved fluids are derived from the same granitic source, and that the numerical simulations carried out by Cline and Bodnar (1991) are applicable. Thus, the interpretation of the plots of fluid salinity vs. mineralization sequence is not simple, and there are a number of possibilities, e.g.:

1) The mineralization is related to multiple granite intrusions, i.e. to the magmatic fluids exsolved during crystallization of these granitic melts; at least five separate different fluid (mineralization) events are recorded by the fluid inclusion in the vein minerals.
2) It is not accounted for the possible dilution by influx of meteoric fluids.
3) The model calculations are only applicable to fluid generation from a calc-alkaline melt and not to highly specialized Li-F granites, which have lower solidus temperatures, different volatile contents and possibly different water solubilities and distribution coefficients of chlorine between melt and exsolving fluid.

Tab. 2. Calculated bulk composition of fluids in primary inclusions in minerals from the vein "Lidernaya", Modoto, Mongolia, based on microthermometric and Raman spectroscopic data and petrographic observations.

Sample No./ Mineral	X (H_2O)	X(CO_2)	X(NaCl)*	X (CH_4)
39/1A massive quartz	(0.82 - 0.97)	(0.02 - 0.16)	(0.008 - 0.013)	(0.001 -0.003)
39/1B cassiterite	0.986 (0.97 - 0.987)	(0 - < 0.02)	0.014 (±0.001)	n.d.
39/1C quartz inclusions in cassiterite	0.967	n.d.	0.033	n.d.
39/2 quartz crystal	(0.85 - 0.97)	(0.02 - 0.14)	(0.005 - 0.013)	** (0.001 - 0.004)
39/3 fluorite	0.997 (0.992 - 0.999)	n.d.	0.003 (0.001 - 0.008)	n.d.
39/4 wolframite	0.969 (0.95 - 0.97)	(0 - < 0.02)	0.031 (±0.001)	n.d.
39/5 cassiterite	0.987 (0.985 - 0.989)	n.d.	0.013 (±0.002)	n.d.
39/6 topaz	0.966 (0.953 - 0.977)	0.027 (0.015 - 0.039)	0.007 (0.005 - 0.008)	(0 - <0.001)

* = includes also electrolytes other than NaCl; ** = includes N_2; n.d. = not detected; (numbers in parentheses) = range in calculated bulk compositions

Tab. 3: Solid inclusions in minerals from the vein "Lidernaya", Modoto, Mongolia.

Sample No./ Mineral	Elements Identified Using SEM-EDS (major elements: bold)	Preliminary Identification	Comments
39/1A massive quartz		rutile? or tourmaline?	euhedral needles
39/1B cassiterite	**Ti** Nb W Fe	(niobian) rutile	apparently unzoned
	Ti Fe Mn	?	with rutile in same inclusion
	Si	quartz	anhedral and corroded, located on outermost growth zones, positively identified using Raman spectroscopy
	Al Si	topaz	euhedral, positively identified using Raman spectroscopy
		muscovite?	anisotropic in transmitted light, euhedral plates, often hexagonal contours
39/2 quartz crystal	**Si Al K**	muscovite	low polishing hardness, very good cleavage in one direction
39/6 topaz	**Si Al K**	muscovite	low polishing hardness, very good cleavage in one direction

Tab. 4. Calculated formation pressures based on formatio n temperature estimates and determined isochore locations of primary inclusions in minerals from the vein "Lidernaya", Modoto, Mongolia.

Sample No./ Mineral	Th(L-V→L) = Tf(min) [°C]	Ph(L-V→L) = Pf(min) [bar]	Tf(est) [°C]	Pf(calc) [bar]
39/1B cassiterite	332	93 (2)	400 - 500	671 - 1522 (3)
39/1C quartz inclusions in cassiterite	465 (C)	463 (1)	500 - 600 650	612 - 1039 (3) 1253 (3)
39/3 fluorite	160	5 (2)	200 180 - 250	694 (3) 349 - 1555 (3)
39/4 wolframite	320	80 (2)	350 - 400	384 - 890 (3)
39/5 cassiterite	334	96 (2)	400 - 500	647 - 1481 (3)
39/6 topaz	326	227 (4)	400 - 500	705 - 1454 (4)

Th(L-V→L) = average liquid-vapor homogenization temperature (total homogenization to the liquid, aqueous phase); Tf(min) = minimum formation temperature; Ph(L-V→L) = homogenization pressure at Th(L-V→L); Pf(min) = minimum formation pressure; Tf(est) = estimated mineral formation temperature; Pf(calc) = calculated formation pressure corresponding to Tf(est); (C) = total homogenization by critical behavior; equations used for calculation of Ph(L-V→L) and Pf(calc): (1) = Knight and Bodnar (1989); (2) = MacFlinCor (Brown and Hagemann, 1989); (3) = Bodnar and Vityk (1994); (4) = Duan et al. (1995)

4) There are two granitic fluid sources, and the pressure at the granite solidus temperature was above 1.5 kbar (although this is not indicated by the geology; furthermore, the intersection of isochore for the primary inclusions in the sample 39/1C and granite solidus indicates an approximate solidus pressure of about 1 to 1.5 kbar during fluid exsolution - at least during the later stages of the paragenetic sequence).
5) The compositions trapped in fluid inclusions in the vein minerals do not reflect the initial X(NaCl) (including other electrolytes) in the fluid exsolved from the melt (due to boiling at high temperatures close to those at the granite solidus?, reactions with the wallrock during ascent?).

The solubility of CO_2 in felsic melts is low at pressures less than about 3 kbar but becomes significantly higher with increasing pressure, particularly in the presence of water (cp. Burnham, 1979). At the vein "Lidernaya", the highest carbon dioxide contents in the fluid were observed in quartz samples from the early wolframite quartz assemblage, but one should not readily draw the conclusion that this fluid was derived from a deeper granitic source; too many variables are not known to properly evaluate the significance of CO_2 concentrations in the hydrothermal fluid (e.g. the amount of carbon dioxide derived from a felsic source, and the H_2O/CO_2 ratios in fluids exsolved from a granitic melt as a function of pressure, initial H_2O/CO_2 ratio, and percentage of melt crystallized).

References

Bodnar R. J. (1993) Revised equation and table for determining the freezing point depression of H_2O-NaCl solutions. *Geochim. Cosmochim. Acta* **57**, 683-684.

Bodnar R. J. and Vityk M. O. (1994) Interpretation of microthermometric data for H_2O-NaCl fluid inclusions. In *Fluid Inclusions in Minerals, Methods and Applications* (ed. B. De Vivo and M. L. Frezotti), pp. 117-130. Virginia Tech, Blacksburg, VA.

Brown P. E. and Hagemann S. G. (1989) MacFlinCor: A computer program for fluid inclusion data reduction and manipulation. In *Fluid Inclusions in Minerals, Methods and Applications* (ed. B. De Vivo and M. L. Frezotti), pp. 231-250. Virginia Tech, Blacksburg, VA.

Burnham C. W. (1979) The importance of volatile constituents. In *The evolution of the igneous rocks* (ed. H. S. Yoder), pp. 439-482. Princeton University Press, Princeton, NJ.

Campbell A. R. and Panter K. S. Comparison of fluid inclusions in coexisting (cogenetic?) wolframite, cassiterite, and quartz from St. Michael's Mount and Cligga Head, Cornwall, England. *Geochim. Cosmochim. Acta* **54**, 673-681.

Cline J. S. and Bodnar R. J. (1991) Can economic porphyry copper mineralization be generated by a typical calc-alkaline melt? Journ. Geophys. Res. 96, No. B5, 8113-8126.

Dandar S. (1990) The evolution of the rare-metal mineralization of the Modoto ore field. Doctoral dissertation, Technical University Ulaanbaatar. (In Russian).

Dandar S., Sizykh V. I., and Dashdavaa S. (1979) The tin-tungsten mineralization of the Modoto ore field. In *Voprosy geologii i metallogenii Vostochnoy Mongolii* **1**, pp. 225-229. (In Russian).

Diamond L. W. (1992) Stability of CO_2 clathrate hydrate + CO_2 liquid + CO_2 vapour + aqueous KCl-NaCl solutions: Experimental determination and application to salinity estimates of fluid inclusions. *Geochim. Cosmochim. Acta* **56**, 273-280.

Diamond L. W. (1994) Salinity of multivolatile fluid inclusions determined from clathrate hydrate stability. *Geochim. Cosmochim. Acta* **58**, 19-41.

Duan Zh., Møller N., and Weare J. H. (1995) Equation of state for the NaCl-H_2O-CO_2 system: Prediction of phase equilibria and volumetric properties. *Geochim. Cosmochim. Acta* **59**, 2869-2882.

Ivanova G. F. (1976) Mineralogy and geochemistry of the tungsten mineralization of Mongolia. Trudy Sovmestnoy Sovetsko-Mongol'skoy nauchno-issledovatel'skoy geologicheskoy ekspedicii **15**. Moscow, Nauka, 260 p. (In Russian).

Knight C. L. and Bodnar R. J. (1989) Synthetic fluid inclusions: IX. Critical PVTX properties of NaCl-H_2O solutions.*Geochim. Cosmochim. Acta* **53**, 3-8.

Lüders V. (1996) Contribution of infrared microscopy to fluid inclusion studies in some opaque minerals (wolframite, stibnite, bournonite): Meallogenetic implications. *Econ. Geol.* **91**, 1462-1468.

Roedder E. (1984) *Fluid Inclusions*. Mineralogical Society of America, Reviews in Mineralogy, Vol. 12, 646 p.

Rosso K. M. and Bodnar R. J. (1995) Microthermometric and Raman spectroscopic detection limits of CO_2 in fluid inclusions and the Raman spectroscopic characterization of CO_2. *Geochim. Cosmochim. Acta* **59**, 3961-3975.

Schmidt C. and Leeder O. (1992) Temperature and pressure conditions during the formation of pegmatites and pneumatolytic tin-tungsten mineralizations in Mongolia. *Neues Jahrbuch Miner. Abh.* **165**, 29-52.

Sterner S. M. and Bodnar R. J. (1984) Synthetic fluid inclusions in natural quartz. I: Compositional types synthesized and applications in experimental geochemistry. *Geochim. Cosmochim. Acta* **48**, 2659-2668.

Swanenberg H. E. C. (1979) Phase equilibria in carbonic systems, and their application to freezing studies of fluid inclusions. Contrib. Mineral. Petrol. **68**, 303-306.

Werre R. W., Jr., Bodnar R. J., Bethke P. M., and Barton P. B., Jr. (1979) A novel gas-flow fluid inclusion heating/freezing stage (abstr.). *Geol. Soc. Amer. Abstr.with Prog.* **11**, 539.